coatings

MDPI

Article

Nanostructured Titanium for Improved Endothelial Biocompatibility and Reduced Platelet Adhesion in Stent Applications

Maria Antonia Llopis-Grimalt [1,2], Maria Antònia Forteza-Genestra [1,2], Víctor Alcolea-Rodriguez [1], Joana Maria Ramis [1,2,*] and Marta Monjo [1,2,*]

[1] Group of Cell Therapy and Tissue Engineering, Department of Fundamental Biology and Health Sciences, Research Institute on Health Sciences (IUNICS), University of the Balearic Islands, 07122 Palma, Spain; mantonia.llopis@uib.es (M.A.L.-G.); maria.forteza@ssib.es (M.A.F.-G.); valcolear@gmail.com (V.A.-R.)

[2] Health Research Institute of the Balearic Islands (IdISBa), 07010 Palma, Spain

* Correspondence: joana.ramis@uib.es (J.M.R.); marta.monjo@uib.es (M.M.); Tel.: +34-971259607 (M.M.)

Received: 10 August 2020; Accepted: 18 September 2020; Published: 22 September 2020

Abstract: Although coronary stents have improved the early and long-term consequences of arterial lesions, the prevention of restenosis and late stent thrombosis is key to prevent a new obstruction of the vessel. Here we aimed at improving the tissue response to stents through surface modification. For that purpose, we used two different approaches, the use of nanostructuration by electrochemical anodization and the addition of a quercitrin (QR) coating to the Ti surface. Four surfaces (Ti, NN, TiQR and NNQR) were characterized by atomic force microscopy, scanning electronic microscopy and contact angle analysis and QR content was evaluated by fluorescent staining. Cell adhesion, cytotoxicity, metabolic activity and nitric oxide (NO) production was evaluated on primary human umbilical cord endothelial cells (HUVECs). Platelet adhesion, hemolysis rate and *Staphylococcus epidermidis* CECT 4184 adhesion at 30 min were analyzed. Nanostructuration induced an increase on surface roughness, and QR coating decreased the contact angle. All surfaces were biocompatible, with no hemolysis rate and lower platelet adhesion was found in NN surfaces. Finally, *S. epidermidis* adhesion was lower on TiQR surfaces compared to Ti. In conclusion, our results suggest that NN structuration could improve biocompatibility of bare metal stents on endothelial cells and reduce platelet adhesion. Moreover, QR coating could reduce bacterial adhesion.

Keywords: stents; surface modification; flavonoids; quercitrin; TiO_2 nanostructure; platelet adhesion; in vitro endothelialization; hemolysis; bacterial adhesion

1. Introduction

Cardiovascular disease is the leading cause of mortality worldwide and its underlying cause is atherosclerosis; a degenerative progressive disease characterized by the accumulation of lipids and immune cell plaques that affect coronary, carotid and other peripheral arteries. The conjunction of immune cells and inflammation with hyperlipidemia (elevated low-density lipoproteins (LDL) levels) influences the plaque rupture and the development of myocardial infarction and stroke [1–3].

Different materials, such as titanium, nitinol, stainless steel and CoCr alloys have been widely used as bare metal stent materials. However, in most cases the use of bare metal stents causes the development of in-stent restenosis, producing the narrowing of the arterial walls due to the vascular smooth muscle cells (SMCs) proliferation [4]. Restenosis consists of the arterial wall healing response to the injury; and the resulting neointima is a combination of SMCs, the extracellular matrix and macrophages [5]. Another less frequent but serious complication of metal stents is infections.

Metal stent infections are associated with an acute inflammation of the arterial wall and vessel thrombosis, and *Staphylococcus aureus* is responsible of about 80% of stent infections. Due to the heterogeneous clinical presentation of stent infections its diagnosis is difficult and there are not many standards for its prevention and treatment [6].

Drug eluting stents (DESs) are used to inhibit the proliferation of smooth muscle cells, decreasing the risk of in-stent restenosis by the delivery of an appropriate concentration of an effective agent locally without systemic toxicity [7]. Usually, this controlled liberation of the therapeutic agent is achieved due to the use of a polymer coating; however, there are some complications associated to the use of polymers, considered as one of the leading causes of late stent thrombosis [8,9]. Thus, the use of a nanostructured surface could provide an alternative for the application of the stent coating without the need of using a polymer.

Titanium oxide (TiO_2) presents an excellent tissue response and although its mechanical properties are not ideal for stents it has been proposed as a surface modification for bare metal stents, providing an hemocompatible surface with improved biocompatibility [10], in which other coatings could also be applied.

Nanoscale topography has shown to control several molecular and cellular processes on its own without the need to change the surface chemical composition. This capacity to modulate cell behavior through topographical features has been observed with different cell types [11,12], showing for example an enhanced endothelial cell attachment and migration on stent surfaces. Furthermore, small pore diameters, less than 100 nm, have proved to promote cell adhesion and differentiation, while bigger diameters promote cell apoptosis [13,14]. Specifically, TiO_2 nanotubes with a 100 nm diameter have shown to decrease HUVEC viability and functionality, highlighting the importance of studying the effect of nanostructures with diameters below 100 nm [15], as the creation of a nanoscale topography on stent surfaces would mimic the vessel structure, improving its biocompatibility [4]. Recent studies suggest that TiO_2 nanotubes improve extracellular matrix secretion and endothelial cell functions while inhibiting vascular smooth muscle cells proliferation, implying that nanostructuration may be a good approach to achieve a faster endothelialization [4].

Another strategy to improve cell differentiation and to avoid bacterial adhesion on implantable devices is to apply a coating with a biomolecule, which can add other beneficial properties to the stent. The coating of TiO_2 with biomolecules, such as fibronectin, has shown to improve HUVEC morphology and nitric oxide (NO) production [15], showing the importance of the evaluation of biomolecule functionalization of stents. Flavonoids are natural phenolic compounds present in the human diet with antioxidant, anti-inflammatory and antimicrobial capacity, with demonstrated beneficial effects on human cells. Quercitrin is a flavonoid that was selected among others in our previous research due to its promotion of gingival cell differentiation and the decrease in *Staphylococcus epidermidis* growth rate [16,17]. In the past years, the potential of poly-phenol (as flavonoids) based coatings in medical devices has risen with applications in different fields such as, cardiovascular stents, dental or orthopedic implants. Titanium surfaces functionalized with quercitrin have shown bone-stimulating, anti-inflammatory and antifibrotic effects in vitro on human bone marrow mesenchymal stem cells and human gingival fibroblasts [18–20].

We aimed to produce a surface that could promote HUVEC function while avoiding platelet and bacterial adhesion. A quercitrin functionalized nanostructured TiO_2 surface was produced and characterized by atomic force microscopy (AFM), scanning electron microscopy (SEM) and contact angle analysis. Then, we analyzed the effect of the surfaces on HUVEC biocompatibility and function, in addition to its hemocompatibility and platelet adhesion. Finally, we evaluated *Staphylococcus epidermidis* adhesion and biofilm formation to the different surfaces.

2. Materials and Methods

2.1. Materials

Machined titanium discs, c.p. grade IV, 6.2 mm diameter and 2 mm height were purchased from Implantmedia (Lloseta, Spain). APTES, quercitrin standard, 2-aminoethyl diphenylborinate (DPBA), polyethylene glycol 4000 (PEG4000) and ammonium fluoride (NH_4F) were purchased from Sigma-Aldrich (St. Louis, MO, USA). Deionized water was obtained from a Millipore system (Billerica, MA, USA). Technical acetone and NaOH were purchased from Fisher Scientific (Madrid, Spain). Reagent grade nitric acid (69.5%), absolute ethanol and anhydrous toluene were purchased from Scharlab (Barcelona, Spain). Hellmanex III solution was purchased from Hellma Hispania (Badalona, Spain).

2.2. Surface Nanostructuration

Titanium discs were polished and cleaned as previously described [21]. Afterwards a nanonet (NN) nanostructure was produced using an Autolab (Metrohm Autolab BV, Utrecht, The Netherlands), the titanium samples as an anode and a platinum electrode (Metrohm Autolab BV, Utrecht, The Netherlands) as a cathode as previously described [22]. Polished titanium discs were anodized in an etilenglycol based electrolyte (0.1 M NH_4F, 8 M H_2O) with a first anodization of 30 min at 35 V and a second one of 10 min at the same voltage. A peeling was done between the first and second anodization using Scotch® MagicTM tape (3M, Maplewood, MN, USA).

2.3. Preparation of Quercitrin-Nanocoated Titanium Surfaces

To obtain the quercitrin-nanocoated titanium surfaces, machined Ti disks and NN-nanostructured Ti disks were used. Machined Ti disks were passivated with 30% HNO_3 for 30 min, rinsed with water until the pH became neutral and left in water for 48 h. NN disks were rinsed with water and left in water for 48 h. Then, all coins were dried under a N_2 flow and aminosilanized with 2% APTES in dry toluene for 24 h under a controlled atmosphere, in order to maintain the relative humidity levels below 10%. After that, the surfaces were chemically functionalized with quercitrin by immersion in a quercitrin hydrate 1 mM aqueous solution (250 µL/coin) at pH 5.5 for 1 h. Then, samples were washed twice with water, dried under a N_2 flow and stored under vacuum at −20 °C until use. The samples were prepared in aseptic conditions.

2.4. Quantification of Quercitrin Grafted to Titanium Surfaces by Fluorescence Spectroscopy

A stock solution of quercitrin standard (500 µM) was prepared in absolute ethanol and stored in aliquots at −80 °C. Standard surfaces with a known amount of quercitrin were prepared by drop casting a volume of stock solution containing a known amount of quercitrin (0.1, 0.25, 0.5, 0.75, 1 or 1.5 nmol) on the surface of passivated Ti coins, which were further allowed to air-dry for 20 min. In a 96-well plate suitable for fluorescence measurements, the samples and standard surfaces were carefully stained with 5 µL of DPBA (22 mM) in methanol and 5 µL of PEG400 (5%, m/v) in ethanol. After 1.5 h, the fluorescence emission spectrum of the samples was acquired, from λem = 500 nm to λem = 700 nm at an excitation wavelength of λex = 480 nm, using a Varian Cary Eclipse fluorescence spectrophotometer with a microplate reader (Agilent Technologies, Santa Clara, CA, USA). A calibration curve was obtained from the maximum fluorescence intensity at λem = 570 nm. Three sample and standard replicates (n = 3) were used in each analysis. Fluorescence images (λex = 450–490 nm) were taken with a Leica DM R (Wetzla, Germany) fluorescence microscope and pseudocolored with Leica software.

2.5. Surface Characterization

The morphology of the different surfaces was analyzed using scanning electron microscopy. Samples were sputter gold coated before SEM analysis. Images were acquired using a scanning electron

microscope (SEM; Hitachi S-3400 N, Krefeld, Germany) using secondary electrons, vacuum conditions and 15 kV of voltage. Images were analyzed using ImageJ software (version 1.49u, National Institutes of Health, Bethesda, MD, USA) to determine the pore diameter.

Topography of the samples was analyzed using an atomic force microscope (VECCO model multicode, VECCO, Plainview, Oyster Bay, NY, USA) in the air tapping mode with a scan size of 10 μm in combination with HQ: NSC35/Al probes (Mikromasch, Lady's Island, SC, USA) with a nominal spring constant of 16 N/m and resonance frequency of 300 kHz.

The static contact angle was calculated by the sessile drop method using a Nikon D3300 (AF-P DX 18-55 mm lent). The contact angle measurements were performed using four samples of each group using 2 μL ultrapure water as the wetting agent. Image analysis was performed using ImageJ software (National Institutes of Health, Bethesda, MD, USA).

2.6. Cell Culture

A pool of human umbilical vein endothelial cells (HUVECs) from different donors (Lonza, Clonetics, Basilea, Switzerland) was used. Lonza assured that cells were ethically and legally obtained, and all donors provided written informed consent. Cells were cultured at 37 °C, 5% CO_2 and maintained in basal medium EBMTM (Lonza, Clonetics, Basilea, Switzerland) supplemented with EGM™ SingleQuots™ (Lonza, Clonetics, Basilea, Switzerland). Cells were seeded in 96-well plates at a density of 7.0×10^3 cells per well for 7 days.

2.7. Bioactivity of Nanostructured Surfaces on HUVEC

Cell adhesion: HUVECs were allowed to adhere for 30 min to the different surfaces. Unbounded cells were removed by washing twice with PBS and cell adhesion was analyzed using the Presto Blue reagent following the manufacturer's protocol (Life Technologies, Carlsbad, CA, USA). Briefly, 10 μL of Presto Blue was added to all samples containing 100 μL of the culture medium. Samples were incubated at 37 °C overnight and then the absorbance of the medium was read at 570 and 600 nm.

Cytotoxicity assay: after 48 h of culture, the presence of lactate dehydrogenase (LDH) in the culture media was used as an index of cell death. Following the manufacturer's instructions (Cytotoxicity Detection kit, Roche Diagnostics, Manheim, Germany), LDH activity was determined spectrophotometrically after 30 min of incubation at room temperature of 50 μL of culture media and 50 μL of the reaction mixture by measuring the oxidation of nicotinamide adenine dinucleotide (NADH) at 490 nm in the presence of pyruvate. Results were presented relative to the LDH activity in the medium of cells cultured in tissue culture plastic (TCP) (low control, 0% of cell death) and of cells growing on TCP treated with surfactant triton X-100 1% (high control, 100% of cell death).

Metabolic activity: total metabolic activity was analyzed at 48 h and 7 days of HUVECs culture using the Presto Blue reagent (Life Technologies, Carlsbad, CA, USA) following the manufacturer's protocol. Presto Blue was added to all samples containing 100 μL of the culture medium. Samples were incubated at 37 °C for 1 h and then the absorbance of the medium was read at 570 and 600 nm.

NO production: NO production was analyzed by measuring the amount of nitrate and nitrite present in the culture media after 48 h and 7 days of incubation using the Nitrate/Nitrite Colorimetric Assay Kit (Cayman Chemical, Ann Arbor, MI, USA). NO production values were normalized by the metabolic activity of each sample.

2.8. Hemocompatibility of the Modified Surfaces

To study the hemocompatibility of the modified surfaces the hemolysis rate was analyzed. In order to do this, 15 mL tubes with 10 mL of PBS were prepared and incubated with the samples for 24 h at 37 °C in orbital agitation at 180 rpm. In addition, tubes with only PBS and no samples were incubated as a negative control, and tubes with MilliQ water as positive control. After the incubation time, 2 mL of blood samples were collected from two different donors and diluted with 2.5 mL of NaCl 0.9%. Then, 200 μL of the diluted samples were added to the 15 mL tube prepared the day before. Samples were

then incubated at 37 °C for 1 h and then centrifuged at 1590× *g* for 5 min. After that, 100 µL of the supernatant were collected and absorbance at 540 nm was read, calculating the hemolysis rate as % versus positive control.

2.9. Platelet Adhesion on the Modified Surfaces

To study platelet adhesion on the modified surfaces, blood from three different donors was collected and centrifuged at 390× *g* for 10 min. Supernatants were collected and mixed to create a platelet pool. After that, 100 µL of the platelet pool were seeded on the implants and cultured for 2 h at 37 °C, 5% CO_2. Then, samples were washed twice with PBS and fixed with a 4% glutaraldehyde solution for 2 h. Finally, samples were washed with MilliQ water and stored at 4 °C with water until use. Samples were dehydrated before the analysis with scanning electron microscopy. Images were acquired using a scanning electron microscope (SEM; Hitachi S-3400 N, Krefeld, Germany) using secondary electrons, vacuum conditions and 15 kV of voltage. Images were analyzed using ImageJ software (version 1.49u) National Institutes of Health, Bethesda, MD, USA) to determine platelet number per implant.

2.10. Bacterial Culture

The bacterial strain used in this study was *Staphylococcus epidermidis* 4184 (CECT, Valencia, Spain; *S. epidermidis*). The strain was maintained in Luria-Bertani (LB) agar plates (Scharlab, Sentmenat, Spain) and cultured in LB broth (Scharlab, Sentmenat, Spain) for 24 h at 37 °C under aerobic conditions in an orbital shaker (180 rpm).

2.11. Bacterial Adhesion and Biofilm Formation on the Modified Surfaces

S. epidermidis adhesion was analyzed after 30 min of incubation with the different surfaces. A bacterial suspension with a 600 nm absorbance of 0.2 corresponding to 7.9×10^7 CFU/mL, estimated from the plates that present between 25 and 300 CFUs, was prepared and 200 µL were seeded on the implants. This bacterial suspension was incubated for 30 min at 37 °C under aerobic conditions. After that, samples were washed twice with PBS in order to eliminate not attached bacteria and then they were sonicated in 500 µL of PBS for 15 min at a frequency of 42 kHz using an ultrasonic bath BRANSON 5510 (Emerson Industrial Automation, Soest, The Netherlands). After sonication, samples were agitated by vortex to detach the bacteria from the surface and serial dilutions were made. These dilutions were seeded in LB agar plates and incubated at 37 °C under aerobic conditions for 48 h. Finally, bacterial colony forming units (CFUs) were estimated from the plates that presented between 25 and 300 CFUs. The results were expressed as CFU/cm^2 of the implant surface.

To analyze the biofilm formation, the same procedure was followed but the samples were incubated with the bacterial suspension for 24 h instead of 30 min. Results were also expressed as CFU/cm^2 of the implant surface.

2.12. Statistical Analysis

All data are presented as the mean value ± standard error of the mean (SEM). A Shapiro–Wilk test was done to assume parametric or non-parametric distributions. Variance homogeneity was analyzed using Levene's test. Parametric data was analyzed by a one-way ANOVA using as post hoc Bonferroni for data with homogeneous variance or Games Howell for data with non-homogeneous variance. Non-parametric data was analyzed by Kruskal–Wallis. To evaluate the effect of nanostructuration or quercitrin functionalization a Student's *t*-test (parametric) or Mann Whitney (non-parametric) was used. Results were considered statistically significant at $p < 0.05$. SPSS software (version 18.0, Chicago, IL, USA) and GraphPad Prism (version 7, La Jolla, CA, USA) were used.

3. Results

3.1. Characterization of Surface Topography and Wettability

An NN surface was obtained with the anodization conditions used, as demonstrated by the SEM images (Figure 1). In addition, coating of the Ti and NN surfaces with quercitrin did not affect its morphology or the pore size, calculated measuring both the length and the width of the pore, since it did not present a circular morphology (Table 1). The data obtained using AFM showed that nanostructured surfaces presented higher Ra and Rq values compared to the non nanostructured ones ($p < 0.001$). No differences on the roughness parameters were added by QR functionalization. In contrast, water contact angle (CA) measurements indicated that although all surfaces were hydrophilic (CA lower than 90°), the contact angle of QR coated samples (TiQR and NNQR) was lower compared to Ti and NN, respectively (QR coated versus non-coated groups; $p < 0.001$).

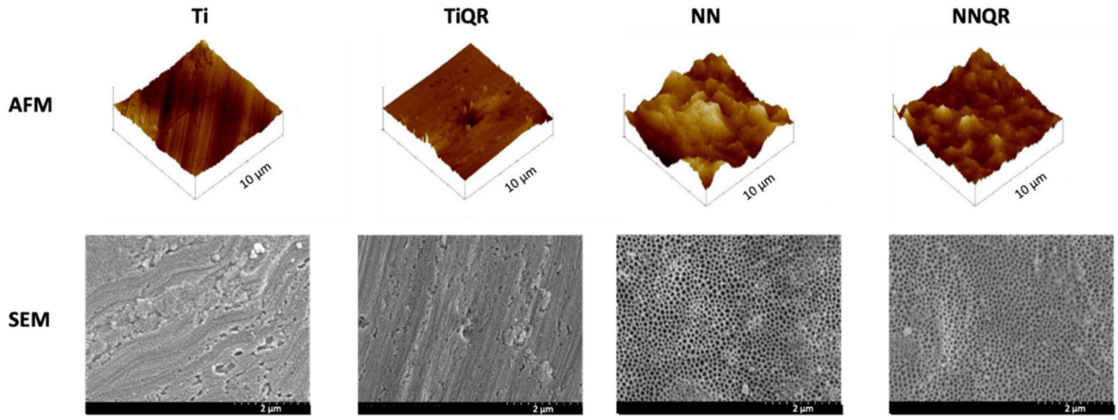

Figure 1. Physical characterization of nanostructured surfaces. Representative AFM (atomic force microscopy) and SEM (scanning electron microscopy) images of the different nanostructured titanium surfaces. Scale bars for each image are shown.

Table 1. Physical characterization of the different titanium surfaces. Values represent the mean ± S.E.M. ° = water contact angle, ⇹ = pore width, ⇳ = pore length, Ra = average roughness, Rq = root mean square. Results were statistically compared by an ANOVA and Bonferroni as post hoc: * $p < 0.05$ versus Ti; $ $p < 0.05$ versus TiQR and # $p < 0.05$ versus NN.

Parameter	Ti	TiQR	NN	NNQR
Contact angle (°)	68.4 ± 1.4	61.3 ± 1.6 *	66.6 ± 0.6	60.5 ± 0.7 *,#
Pore size (nm) ⇹	-	-	84.2 ± 4.2	79.8 ± 2.5
Pore size (nm) ⇳	-	-	55.8 ± 2.8	51.0 ± 1.13
Ra (nm)	37.2 ± 5.9	25.0 ± 3.6	61.8 ± 5.3 *, $	46.8 ± 7.2 $
Rq (nm)	46.8 ± 7.2	34.7 ± 4.2	78.4 ± 6.6 *, $	70.6 ± 8.8 $

3.2. Physical Characterization of Quercitrin Nanocoated Surfaces

A homogeneous quercitrin coating was obtained on both Ti and NN surfaces as demonstrated by the fluorescence coating. The fluorescence microscope images showed higher fluorescence in NN-QR surfaces compared to TiQR, indicating a higher amount (2.5-fold) of quercitrin linked to the nanostructured surfaces, as shown in Figure 2.

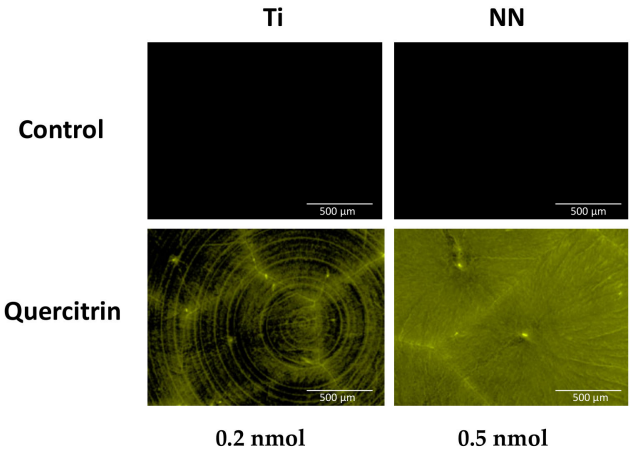

Figure 2. Quercitrin functionalized titanium surfaces staining. Representative fluorescence images of the quercitrin functionalized titanium surfaces after a fluorescence staining. 0.2 ± 0.1 nmol of QR were immobilized for the TiQR group while up to 0.5 ± 0.2 nmol of QR could be detected for the NNQR group.

3.3. Bioactivity of the Quercitrin Functionalized Nanostructured Surfaces on HUVEC

HUVECs were used as a vascular endothelial cell in vitro model to determine the potential effects of the nanostructuration and quercitrin coating of surfaces on endothelial cells.

HUVEC adhesion on the different surfaces was analyzed 30 min after seeding (Figure 3A), showing a higher adhesion on the NN surface compared to TiQR (24.7% increase) and a lower adhesion on NNQR compared to NN surfaces (34.4% decrease). After 48 h of culture, cytotoxicity levels of cells cultured on all surfaces were lower than 30% (Figure 3B), which is the limit for biological evaluation of medical devices (ISO 10993-5:2009). Furthermore, all the modified surfaces showed improved biocompatibility compared to Ti, though for the NNQR statistical significance was not reached. Next, we evaluated the effect of the surfaces on HUVEC metabolic activity at 48 h and 7 days of culture (Figure 3C,D). An effect of quercitrin functionalization was observed on metabolic activity, being higher on cells cultured on the quercitrin coated surfaces (TiQR and NNQR) compared to Ti after 48 h (15.6% and 46.7% increase respectively) and 7 days of incubation (57.2% and 78.1% increase respectively).

Furthermore, NO production was analyzed to study the effect of the surface modification on HUVEC differentiation after 48 h and 7 d of incubation (Figure 4). NO levels in the cell culture media were corrected by the metabolic activity levels of each specific sample. After 48 h of incubation lower NO production was observed in cells cultured on the quercitrin coated surfaces, being significant for both the TiQR and NNQR group compared to Ti (42.72% and 42.72% decrease respectively), and an effect of quercitrin was observed. After 7 days of incubation a decrease in NO production can be observed in all groups (TiQR, NN and NNQR) compared to Ti, although statistical significance was only achieved in NNQR compared to Ti and TiQR. In addition, an effect of nanostructuration and quercitrin was observed, showing a lower NO production in cells cultured onto nanostructured and quercitrin coated surfaces.

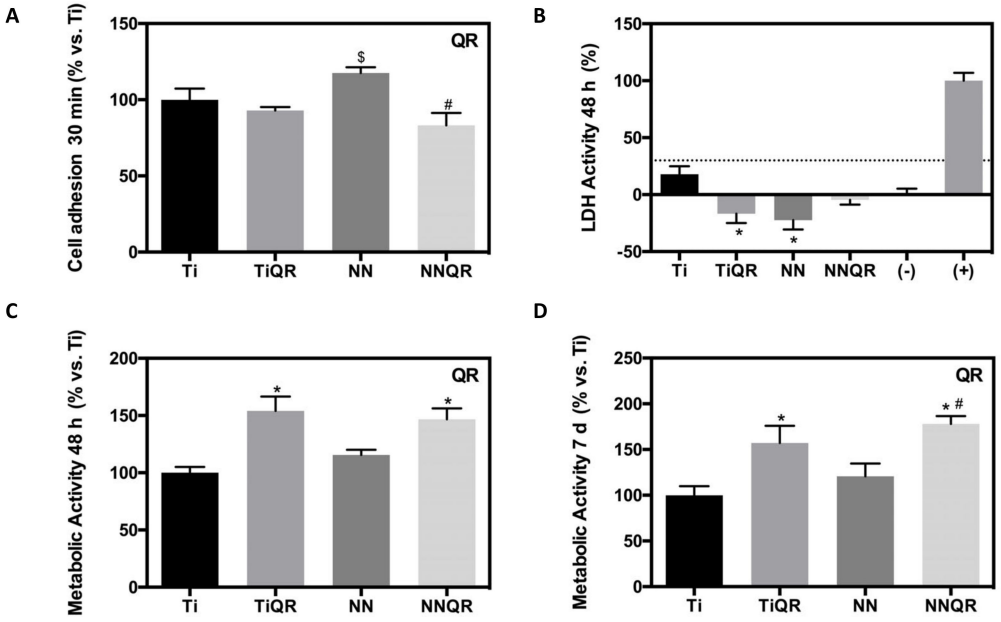

Figure 3. Surface bioactivity on human umbilical vein endothelial cells (HUVECs). (**A**) Cell adhesion to the surfaces after 30 min of incubation, expressed as % vs. Ti ($n = 6$). (**B**) Cytotoxicity of cells cultured on the different surfaces, measured as LDH activity; cells cultured on (TCP) are considered (−) an cells treated with Triton 100X 1% are considered (+; $n = 7$). (**C**) Metabolic activity of cells cultured on the different surfaces for 48 h; results are expressed as % vs. Ti ($n = 7$). (**D**) Metabolic activity of cells cultured on the different surfaces for 7 days ($n = 7$). Values represent the mean ± S.E.M. Results were statistically compared by an ANOVA and Bonferroni as a post hoc for LDH activity and metabolic activity 7 d, by ANOVA and Games Howell as a post hoc for cell adhesion and by Kruskal–Wallis for metabolic activity 48 h. * $p < 0.05$ versus Ti; # $p < 0.05$ versus NN and \$ $p < 0.05$ versus TiQR. QR indicates the effect of quercitrin functionalization ($p < 0.05$), as assessed by Student's *t*-test for cell adhesion, LDH activity and metabolic activity 7 d and by Mann–Whitney for metabolic activity 48 h.

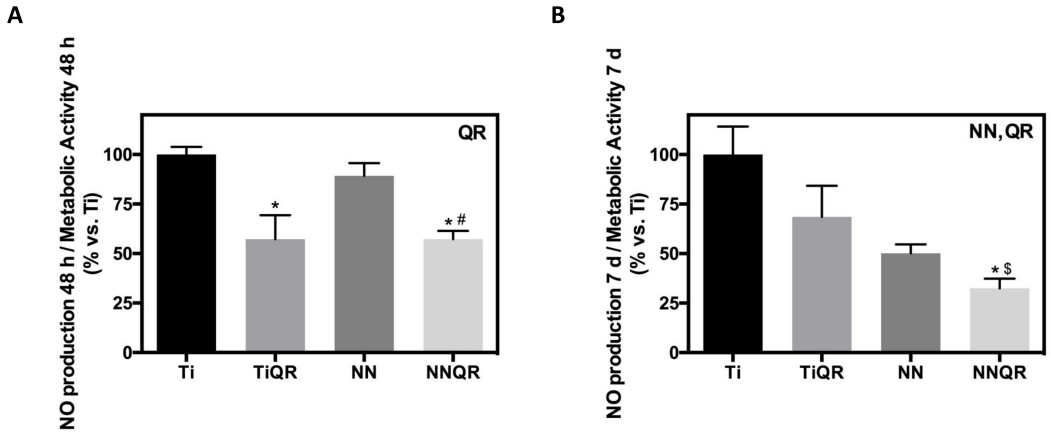

Figure 4. HUVEC NO production corrected by metabolic activity levels. (**A**) NO production corrected by metabolic activity levels after 48 h of incubation; results are expressed as % vs. Ti ($n = 7$). (**B**) NO production corrected by metabolic activity after 7 d of incubation; results are expressed as % vs. Ti. Values represent the mean ± S.E.M ($n = 7$). Results were statistically compared by an ANOVA and Bonferroni as a post hoc for NO production 48 h and Kruskal–Wallis for NO production 7d. * $p < 0.05$ versus Ti; \$ $p < 0.05$ versus TiQR; # $p < 0.05$ versus NN. QR indicates effect of quercitrin functionalization ($p < 0.05$); NN indicates effect of nanostructuration ($p < 0.05$) as assessed by a Student's *t*-test for NO production 48 h or Mann–Whitney for NO production 7 d.

3.4. Hemocompatibility of the Nanostructured Quercitrin Functionalized Nanostructured Surfaces

To test the hemocompatibility of the surfaces, a hemolysis rate test and a platelet adhesion experiment were performed (Figure 5). All the surfaces tested showed no hemolysis rate when tested using blood collected from different donors. In addition, platelet adhesion was lower in nanostructured surfaces (NN and NNQR) compared to Ti (77.1% and 48.1% decrease respectively) and TiQR (93.9% and 64.9% decrease respectively). Quercitrin coating of the surfaces did not decrease platelet adhesion, in contrast, NNQR surface showed a higher platelet adhesion than NN, although this did not reach statistical significance. In this case, the nanostructuration of the surfaces had a greater impact than the quercitrin coating on the hemocompatibility of the surfaces.

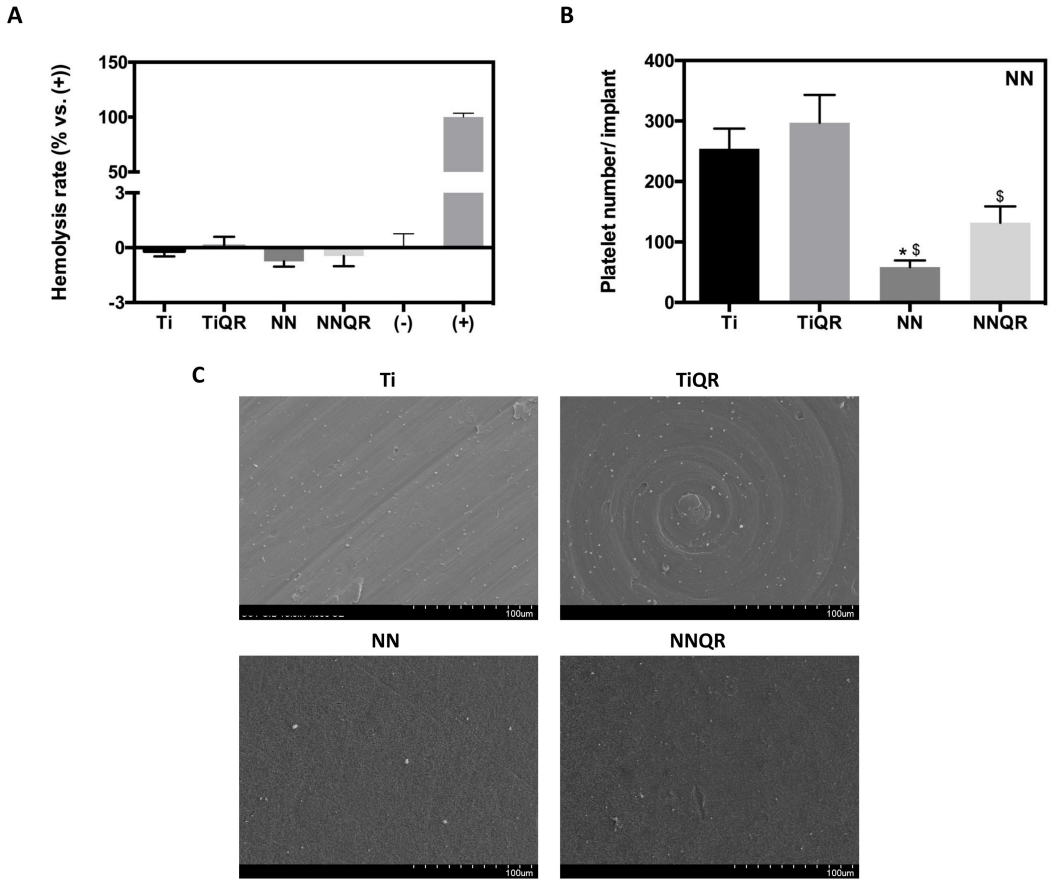

Figure 5. Hemocompatibility and platelet adhesion. (**A**) Hemolysis rate induced by the surfaces after 1 h of incubation, expressed as % vs. (+) that was set to 100%. Blood incubated with water is considered (+), and blood incubated with PBS is considered (−) (n = 6). (**B**) Platelet adhesion after 2 h on the different surfaces (n = 8). (**C**) Representative SEM images of human platelets adhered to the different surfaces. Values represent the mean ± S.E.M. Results were statistically compared by Kruskal–Wallis. * $p < 0.05$ versus Ti; $ $p < 0.05$ versus TiQR. NN indicates the effect of nanostructuration ($p < 0.05$) as assessed by Mann–Whitney.

3.5. Bacterial Adhesion and Biofilm Formation on the Nanostructured Quercitrin Functionalized Surfaces

S. epidermidis adhesion on the different surfaces was tested after 30 min of seeding (Figure 6A). Bacterial adhesion was lower on TiQR surfaces compared to Ti (50.2% decrease) and there was no difference between NN and NNQR compared to Ti. Although there was no decrease of bacterial adhesion on these surfaces, it is important to mention the fact that there was no increase despite their higher surface roughness on nanostructured groups. No differences were observed in the ability of the bacteria to create a biofilm after 24 h among the groups (Figure 6B).

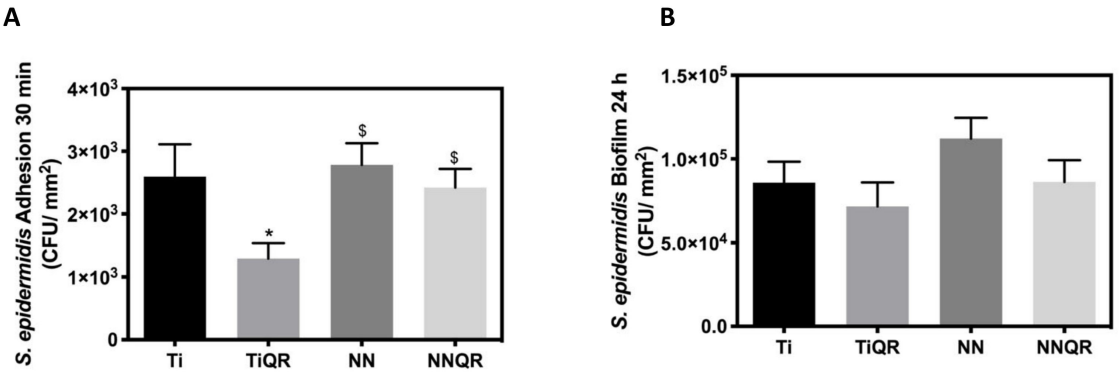

Figure 6. *Staphylococcus epidermidis* adhesion and biofilm formation. (**A**) *S. epidermidis* adhesion after 30 min of incubation. (**B**) *S. epidermidis* biofilm formation after 24 h of incubation on the surfaces. Values represent the mean ± S.E.M., (n = 6). Three different experiments were performed in duplicate. Results were statistically compared by Kruskal–Wallis for bacterial adhesion and an ANOVA and Bonferroni as a post hoc for biofilm formation. * $p < 0.05$ versus Ti; $ $p < 0.05$ versus TiQR.

4. Discussion

Cardiovascular diseases represent one of the leading causes of premature death and bring a tremendous economic burden [23]. Ti and its alloys are widely used for biomedical implants, such coronary bare metal stents, which usually fail due to in-stent restenosis. In this work, we tried two different approaches to improve the outcome of this material: the use of nanostructuration and the addition of a quercitrin coating to the Ti surface. Although we failed to find a synergic effect, we found on one hand that nanostructuration decreased platelet adhesion and in turn decreased the risk of thrombosis, while improving the biocompatibility of endothelial cells; and on the other hand we found that QR coating decreased bacterial adhesion, thus decreasing the risk of infection.

The characterization of the nanostructures produced in the present study allowed the determination of roughness, contact angle and geometry of the pores that could influence the cell and bacterial response. Roughness was similar when compared to other studies [24], but geometry and hydrophilicity of these surfaces showed some differences. Thus, our nanonet structure differed in morphology and geometry compared to nanopores in other studies [25], showing also a higher hydrophilicity compared to our study. The use of a nanostructured TiO_2 surface of the stent allows the creation of a surface that mimics the vascular walls, as it possesses nanostructured features, such as collagen and elastin of the endothelial cellular matrix. Previous studies have described that the presence of nanostructures on the surface enhances stent endothelialization preventing thrombosis [26–28]. However, in other studies nanostructuration of Ti surfaces did not show any effect on platelet aggregation compared with Ti before endothelialization [10,29]. In our study, all surfaces tested were hemocompatible, showing a low hemolysis rate, and nanostructured surfaces (NN and NNQR) presented significantly lower platelet adhesion compared to the non-nanostructured ones (Ti and TiQR). This result supports that our nanostructured surface could help prevent stent related thrombosis, as nanostructuration prevents platelet aggregation on the surface.

Another important aspect when developing new high-risk medical devices such as coronary stents is the biocompatibility, which follows ISO 10993:5. All our new surfaces tested were biocompatible, and the nanostructured surface (NN) showed the best biocompatibility results on endothelial cells of all the groups, proving that TiO_2 coatings possess excellent biocompatibility, in agreement with other reports [22]. In regard to cell adhesion, some studies have shown a lower cell count after one day of culture on Ti nanotubular surfaces with a 110 nm diameter [15], showing the importance of evaluating nanostructured surfaces with smaller diameters, like the ones produced in this study, with an average size of 84.2 ± 4.2 nm × 55.8 ± 2.8 nm. Although our results show a higher cell adhesion in the NN group, we failed to find a significant difference with nanostructuration.

Another aspect evaluated in this work is related to the differentiation of the HUVEC cells, which can be measured with the release of nitric oxide. Nitric oxide synthase (NOS-3) is present in the vascular endothelium and synthetizes nitric oxide (NO) from L-arginine. NO has an atheroprotective, thromboresistant and vasodilator role in the endothelium. Therefore, the dysfunction of this pathway contributes to various cardiovascular disorders such as hypertension, atherosclerosis, intimal hyperplasia or restenosis [30,31]. Different studies have reported an increase in NO production of HUVEC cultured on nanostructured surfaces compared to cells cultured on Ti [10,15]. However, we observe a decrease in NO production of cells cultured on NNQR surfaces after 48 h and 7 d compared to Ti, and after 7 days an effect of nanostructuration and QR coating was observed, leading to a decrease in NO production, which could be related to a higher cell proliferation and a lower cell differentiation. It should be kept in mind that both, micro and nanostructuration may affect the cellular response to the surfaces, in fact, in a previous study, we could demonstrate that NN surfaces induced an oriented alignment of both human gingival fibroblasts and human bone marrow mesenchymal stem cells, leading in turn to an improved expression of differentiation markers [22,32]. In a previous paper, we also showed that gingival fibroblast cells grew aligned to machined surfaces and disorderly on the polished ones [32].

Finally, bacterial adhesion to the modified surfaces was studied. Infections following the placement of cardiovascular devices is rare but it can be life-threatening and difficult to treat [6,33], and the increase of surface roughness induced by the nanostructuration process could favor bacterial adhesion, as reported in other studies [34]. Nevertheless, *S. epidermidis* adhesion was equal in nanostructured and Ti surfaces.

In regard to the second strategy with the addition of a quercitrin coating, we have previously fully characterized the coating and demonstrated that the flavonoid quercitrin could be an excellent choice for implant coating due to its multifunctional properties [18,19,35,36]. Most flavonoids are considered nontoxic and are present in plant-derived foods and present anti-inflammatory, antimutagenic and anticarcinogenic properties [37]. In previous studies, we have demonstrated that quercitrin coating presents good biocompatibility, osteopromotive, anti-inflammatory and antibacterial activity [18,19,35,36]. Here, we proved that quercitrin could also be applied as a coating for bare metal stents, and combined with the nanostructured surface, to overcome the main drawbacks of DES. In fact, the coating procedure was adapted and proved to perform successfully on the nanostructured surfaces, showing a higher amount of linked flavonoid. In addition, it is important to mention that the QR coating did not alter the nanostructure morphology or topography, in agreement with previous studies where it was demonstrated that the coating did not affect surface roughness [18,19]. The water contact angle was the only parameter affected by the QR coating, and this decrease was expected due to the presence of the biomolecule on the implant surface. The use of a coating that is covalently linked to the surface, as demonstrated by FTIR spectroscopy and XPS in previous studies [18,19], could provide an alternative to the use of a polymer, which is considered as one of the leading causes of late stent thrombosis in DES [8,9]. Similar to previous reports [19,35], QR coated surfaces were also biocompatible on HUVEC cells, and remarkably showed higher metabolic activity in all evaluated time points, similar to other studies with mesenchymal stem cells [18,19]. This result is promising since a rapid endothelialization of the stent surface is very important in order to avoid thrombosis, a major complication of DES. After 48 h of incubation with the surfaces, NO production levels show an opposite profile compared to the metabolic activity. This could indicate that the QR coating is promoting cell proliferation rather than initiating cell differentiation. However, after 7 days of incubation a tendency of lower NO production in the nanostructured surfaces (NN and NNQR) was found. In the case of NNQR surface, this result correlated again with the metabolic activity profile, being this surface the one that stimulated a higher cell proliferation and a lower cell differentiation.

On the other hand, QR coating did not seem to have an important impact on hemocompatibility of the different surfaces, as no differences were observed on the hemolysis rate and platelet adhesion,

despite flavonoids having been reported to present antiplatelet effects and to be able to inhibit platelet aggregation [38,39].

Last, due to the clinical implications of implant-related infections and with the rising of antimicrobial resistance, there is a need to develop antibacterial coatings with other molecules rather than antibiotics. Plants synthesize flavonoids in response to microbial infection and they have also been proposed as resistance-modifying agents that can act synergically with antibiotics against resistant bacterial strains [37]. In previous studies in our research group, TiQR surfaces significantly decreased *Streptococcus mutans* adhesion compared to Ti [20], similar to the present results with *S. epidermidis*. Therefore, this type of surface could help to prevent intravascular bare metal stent infections, which are rare but a serious complication, and often leads to emergency surgery. Moreover, bacteria commonly found in skin flora such as *S. aureus* and *S. epidermidis* are the most common bacterial causes of both vascular graft and stent infections [40], from which we reported an effect. However, future studies in elucidating the effects of QR on different bacterial may be useful for optimizing the efficiency and feasibility of the QR-coated biomaterials in biomedical applications.

The fact that these studies were performed using Ti discs represent a limitation in the study, together with the fact that HUVEC behavior and hemocompatibility were tested in vitro in conditions that are far from the in vivo situation. In future studies, nanostructuration or quercitrin coating should be performed on a final medical device using coronary Ti stents, and including mechanical testing in the studies using various modes of failing such as bending, torsion, tensile, crushing, abrasion and fatigue to analyze if any of these modifications are affecting the mechanical properties and durability. Finally, an in vivo study with a validated animal model under aseptic and infected conditions is necessary to determine the histological effects of the coatings and its hemocompatibility in an in vivo environment.

5. Conclusions

Nanostructuration of Ti surfaces has shown improved biocompatibility on endothelial cells and hemocompatibility, which could represent a good option as a surface modification for bare metal stents to produce a rapid re-endothelialization and prevent thrombosis. Moreover, the use of quercitrin functionalization on Ti implants has shown lower bacterial adhesion, which could reduce the risk of bacterial infection.

Author Contributions: Conceptualization, M.M., J.M.R., and M.A.L.-G.; methodology, M.M., J.M.R., and M.A.L.-G.; validation, M.M. and J.M.R.; formal analysis, M.M., J.M.R., and M.A.L.-G.; investigation, M.A.L.-G., M.A.F.-G., and V.A.-R.; resources, M.M. and J.M.R.; data curation, M.A.L.-G.; writing—original draft preparation, M.A.L.-G.; writing—review and editing, M.M., J.M.R., and M.A.L.-G.; supervision, M.M. and J.M.R.; project administration, M.M. and J.M.R.; funding acquisition, M.M. and J.M.R. All authors have read and agreed to the published version of the manuscript.

Funding: This research was funded by a grant from the Osteology Foundation (Switzerland; 13-069), by the Ministerio de Educación Cultura y Deporte (contract to M.A. L.G; FPU15/03412), by Instituto de Salud Carlos III, co-funded by the ESF European Social Fund and the ERDF European Regional Development Fund (contract to J.M.R.; MS16/00124), Ministerio de Economía y Competividad (contract to M.M.; IEDI-2017-00941), and the Institut d'Investigació Sanitària de les Illes Balears (ITS2018-002-TALENT PLUS JUNIOR PROGRAM, JUNIOR18/01)

Acknowledgments: The authors thank Ferran Hierro and Joan Cifre, (UIB) for their technical contribution with SEM and AFM, respectively.

Conflicts of Interest: The authors declare no conflict of interest.

References

1. Lusis, A.J. Atherosclerosis Aldons. *Nature* **2010**, *407*, 233–241. [CrossRef] [PubMed]
2. Schaftenaar, F.; Frodermann, V.; Kuiper, J.; Lutgens, E. Atherosclerosis: The interplay between lipids and immune cells. *Curr. Opin. Lipidol.* **2016**, *27*, 209–215. [CrossRef] [PubMed]
3. O'Connell, B.M.; McGloughlin, T.M.; Walsh, M.T. Factors that affect mass transport from drug eluting stents into the artery wall. *Biomed. Eng. Online* **2010**, *9*, 6–8. [CrossRef] [PubMed]

4. Mohan, C.C.; Sreerekha, P.R.; Divyarani, V.V.; Nair, S.; Chennazhi, K.; Menon, D. Influence of titania nanotopography on human vascular cell functionality and its proliferation in vitro. *J. Mater. Chem.* **2012**, *22*, 1326–1340. [CrossRef]
5. Costa, M.A.; Simon, D.I. Molecular basis of restenosis and drug-eluting stents. *Circulation* **2005**, *111*, 2257–2273. [CrossRef]
6. Zhang, K.; Liu, T.; Li, J.-A.; Chen, J.-Y.; Wang, J.; Huang, N. Surface modification of implanted cardiovascular metal stents: From antithrombosis and antirestenosis to endothelialization. *J. Biomed. Mater. Res. Part A* **2014**, *102*, 588–609. [CrossRef]
7. Htay, T.; Liu, M.W. Drug-eluting stent: A review and update. *Vasc. Health Risk Manag.* **2005**, *1*, 263–276. [CrossRef]
8. Bedair, T.M.; Min, I.J.; Park, W.; Joung, Y.K.; Han, D.K. Sustained drug release using cobalt oxide nanowires for the preparation of polymer-free drug-eluting stents. *J. Biomater. Appl.* **2018**, *33*, 352–362. [CrossRef]
9. Lee, C.H.; Hsieh, M.J.; Liu, K.S.; Cheng, C.W.; Chang, S.H.; Liu, S.J.; Wang, C.J.; Hsu, M.Y.; Hung, K.C.; Yeh, Y.H.; et al. Promoting vascular healing using nanofibrous ticagrelor-eluting stents. *Int. J. Nanomed.* **2018**, *13*, 6039–6048. [CrossRef]
10. Mohan, C.C.; Chennazhi, K.P.; Menon, D. In vitro hemocompatibility and vascular endothelial cell functionality on titania nanostructures under static and dynamic conditions for improved coronary stenting applications. *Acta Biomater.* **2013**, *9*, 9568–9577. [CrossRef]
11. Dobbenga, S.; Fratila-Apachitei, L.E.; Zadpoor, A.A. Nanopattern-induced osteogenic differentiation of stem cells—A systematic review. *Acta Biomater.* **2016**, *46*, 3–14. [CrossRef]
12. Metavarayuth, K.; Sitasuwan, P.; Zhao, X.; Lin, Y.; Wang, Q. Influence of Surface Topographical Cues on the Differentiation of Mesenchymal Stem Cells in Vitro. *ACS Biomater. Sci. Eng.* **2016**, *2*, 142–151. [CrossRef]
13. Park, J.; Bauer, S.; Von Der Mark, K.; Schmuki, P. Nanosize and Vitality: TiO_2 Nanotube Diameter Directs Cell Fate. *Nano Lett.* **2007**, *7*, 1686–1691. [CrossRef] [PubMed]
14. Park, J.; Bauer, S.; Schlegel, K.A.; Neukam, F.W.; von der Mark, K.; Schmuki, P. TiO_2 Nanotube Surfaces: 15 nm-An Optimal Length Scale of Surface Topography for Cell Adhesion and Differentiation. *Small* **2009**, *5*, 666–671. [CrossRef] [PubMed]
15. Jin, Z.; Yan, X.; Liu, G.; Lai, M. Fibronectin modified TiO_2 nanotubes modulate endothelial cell behavior. *J. Biomater. Appl.* **2018**, *33*, 44–51. [CrossRef]
16. Gómez-Florit, M.; Monjo, M.; Ramis, J.M. Identification of quercitrin as a potential therapeutic agent for periodontal applications. *J. Periodontol.* **2014**, *85*, 966–974. [CrossRef] [PubMed]
17. Satué, M.; Arriero, M.D.M.; Monjo, M.; Ramis, J.M. Quercitrin and Taxifolin stimulate osteoblast differentiation in MC3T3-E1 cells and inhibit osteoclastogenesis in RAW 264.7 cells. *Biochem. Pharmacol.* **2013**, *86*, 1476–1486. [CrossRef]
18. Córdoba, A.; Monjo, M.; Hierro-Oliva, M.; González-Martín, M.L.; Ramis, J.M. Bioinspired Quercitrin Nanocoatings: A Fluorescence-Based Method for Their Surface Quantification, and Their Effect on Stem Cell Adhesion and Differentiation to the Osteoblastic Lineage. *ACS Appl. Mater. Interfaces* **2015**, *7*, 16857–16864. [CrossRef]
19. Córdoba, A.; Satué, M.; Gómez-Florit, M.; Hierro-Oliva, M.; Petzold, C.; Lyngstadaas, S.P.; González-Martín, M.L.; Monjo, M.; Ramis, J.M. Flavonoid-Modified Surfaces: Multifunctional Bioactive Biomaterials with Osteopromotive, Anti-Inflammatory, and Anti-Fibrotic Potential. *Adv. Healthc. Mater.* **2015**, *4*, 540–549. [CrossRef]
20. Gomez-Florit, M.; Pacha-Olivenza, M.A.; Fernández-Calderón, M.C.; Córdoba, A.; González-Martín, M.L.; Monjo, M.; Ramis, J.M. Quercitrin-nanocoated titanium surfaces favour gingival cells against oral bacteria. *Sci. Rep.* **2016**, *6*, 22444. [CrossRef]
21. Lamolle, S.F.; Monjo, M.; Lyngstadaas, S.P.; Ellingsen, J.E.; Haugen, H.J. Titanium implant surface modification by cathodic reduction in hydrofluoric acid: Surface characterization and in vivo performance. *J. Biomed. Mater. Res. Part A* **2009**, *88*, 581–588. [CrossRef] [PubMed]
22. Llopis-Grimalt, M.A.; Amengual-Tugores, A.M.; Monjo, M.; Ramis, J.M. Oriented cell alignment induced by a nanostructured titanium surface enhances expression of cell differentiation markers. *Nanomaterials* **2019**, *9*, 1661. [CrossRef] [PubMed]

23. Heidenreich, P.A.; Trogdon, J.G.; Khavjou, O.A.; Butler, J.; Dracup, K.; Ezekowitz, M.D.; Finkelstein, E.A.; Hong, Y.; Johnston, S.C.; Khera, A.; et al. Forecasting the future of cardiovascular disease in the United States: A policy statement from the American Heart Association. *Circulation* **2011**, *123*, 933–944. [CrossRef]
24. Kulkarni, M.; Patil-Sen, Y.; Junkar, I.; Kulkarni, C.V.; Lorenzetti, M.; Iglič, A. Wettability studies of topologically distinct titanium surfaces. *Colloids Surf. B Biointerfaces* **2015**, *129*, 47–53. [CrossRef]
25. Liu, G.; Du, K.; Wang, K. Surface wettability of TiO_2 nanotube arrays prepared by electrochemical anodization. *Appl. Surf. Sci.* **2016**, *388*, 313–320. [CrossRef]
26. Karagkiozaki, V.; Karagiannidis, P.G.; Kalfagiannis, N.; Kavatzikidou, P.; Patsalas, P.; Georgiou, D.; Logothetidis, S. Novel nanostructured biomaterials: Implications for coronary stent thrombosis. *Int. J. Nanomed.* **2012**, *7*, 6063–6076.
27. Choudhary, S.; Berhe, M.; Haberstroh, K.M.; Webster, T.J. Increased endothelial and vascular smooth muscle cell adhesion on nanostructured titanium and CoCrMo. *Int. J. Nanomed.* **2006**, *1*, 41–49. [CrossRef] [PubMed]
28. Maguire, P.D.; McLaughlin, J.A.; Okpalugo, T.I.T.; Lemoine, P.; Papakonstantinou, P.; McAdams, E.T.; Needham, M.; Ogwu, A.A.; Ball, M.; Abbas, G.A. Mechanical stability, corrosion performance and bioresponse of amorphous diamond-like carbon for medical stents and guidewires. *Diam. Relat. Mater.* **2005**, *14*, 1277–1288. [CrossRef]
29. Achneck, H.E.; Jamiolkowski, R.M.; Jantzen, A.E.; Haseltine, J.M.; Lane, W.O.; Huang, J.K.; Galinat, L.J.; Serpe, M.J.; Lin, F.H.; Li, M.; et al. The biocompatibility of titanium cardiovascular devices seeded with autologous blood-derived endothelial progenitor cells. EPC-seeded antithrombotic Ti Implants. *Biomaterials* **2011**, *32*, 10–18. [CrossRef]
30. O'Connor, D.M.; O'Brien, T. Nitric oxide synthase gene therapy: Progress and prospects. *Expert Opin. Biol. Ther.* **2009**, *9*, 867–878. [CrossRef]
31. Vallance, P.; Hingorani, A. Endothelial nitric oxide in humans in health and disease. *Int. J. Exp. Pathol.* **1999**, *80*, 291–303. [CrossRef] [PubMed]
32. Gómez-Florit, M.; Ramis, J.M.; Xing, R.; Taxt-Lamolle, S.; Haugen, H.J.; Lyngstadaas, S.P.; Monjo, M. Differential response of human gingival fibroblasts to titanium- and titanium-zirconium-modified surfaces. *J. Periodontal Res.* **2014**, *49*, 425–436. [CrossRef] [PubMed]
33. Lejay, A.; Koncar, I.; Diener, H.; Vega de Ceniga, M.; Chakfé, N. Post-operative Infection of Prosthetic Materials or Stents Involving the Supra-aortic Trunks: A Comprehensive Review. *Eur. J. Vasc. Endovasc. Surg.* **2018**, *56*, 885–900. [CrossRef]
34. Teughels, W.; Van Assche, N.; Sliepen, I.; Quirynen, M. Effect of material characteristics and/or surface topography on biofilm development. *Clin. Oral Implants Res.* **2006**, *17* (Suppl. S2), 68–81. [CrossRef]
35. Llopis-Grimalt, M.A.; Arbós, A.; Gil-Mir, M.; Mosur, A.; Kulkarni, P.; Salito, A.; Ramis, J.M.; Monjo, M. Multifunctional Properties of Quercitrin-Coated Porous Ti-6Al-4V Implants for Orthopaedic Applications Assessed In Vitro. *J. Clin. Med.* **2020**, *9*, 855. [CrossRef] [PubMed]
36. Córdoba, A.; Manzanaro-Moreno, N.; Colom, C.; Rønold, H.J.; Lyngstadaas, S.P.; Monjo, M.; Ramis, J.M. Quercitrin Nanocoated Implant Surfaces Reduce Osteoclast Activity In Vitro and In Vivo. *Int. J. Mol. Sci.* **2018**, *19*, 3319. [CrossRef]
37. Górniak, I.; Bartoszewski, R.; Króliczewski, J. Comprehensive review of antimicrobial activities of plant flavonoids. *Phytochem. Rev.* 2019; 18, 241–272.
38. Faggio, C.; Sureda, A.; Morabito, S.; Sanches-Silva, A.; Mocan, A.; Nabavi, S.F.; Nabavi, S.M. Flavonoids and platelet aggregation: A brief review. *Eur. J. Pharmacol.* **2017**, *807*, 91–101. [CrossRef]
39. Guerrero, J.A.; Lozano, M.L.; Castillo, J.; Benavente-García, O.; Vicente, V.; Rivera, J. Flavonoids inhibit platelet function through binding to the thromboxane A2 receptor. *J. Thromb. Haemost.* **2005**, *3*, 369–376. [CrossRef]
40. Bosman, W.M.P.F.; Borger Van Der Burg, B.L.S.; Schuttevaer, H.M.; Thoma, S.; Hedeman Joosten, P.P. Infections of intravascular bare metal stents: A case report and review of literature. *Eur. J. Vasc. Endovasc. Surg.* **2014**, *47*, 87–99. [CrossRef]